PHYSICAL REVIEW B **87**, 245314 (2013)

Steering photon statistics in single quantum dots: From one- to two-photon emission

G. Callsen,* A. Carmele, G. Hönig, C. Kindel, J. Brunnmeier, M. R. Wagner, E. Stock, J. S. Reparaz, A. Schliwa, S. Reitzenstein, A. Knorr, and A. Hoffmann

Institut für Festkörperphysik, Technische Universität Berlin, Hardenbergstraße 36, 10623 Berlin, Germany

S. Kako and Y. Arakawa

Institute of Industrial Science, University of Tokyo, 4-6-1 Komaba, Meguro-ku, Tokyo 153-8505, Japan

(Received 4 October 2012; revised manuscript received 16 May 2013; published 26 June 2013)

We present a combined experimental and theoretical study of two-photon emission from the biexciton cascade in single GaN quantum dots. By changing the biexciton binding energy, pump power, and temperature, the balance between the one- and two-photon decay processes is controlled in this four-level system, which drastically affects the photon statistics of the resulting emission. As the most pronounced feature of this interplay we observe a bunching phenomenon and a transition from sub- to super-Poissonian photon statistics, originating from the complex nature of the biexciton cascade. This work highlights how photon statistics can be steered between one- and two-photon processes towards an increased, bunched two-photon emission probability up to 50 K with the perspective for efficient photon pair generation in the UV spectral range.

DOI: 10.1103/PhysRevB.87.245314 PACS number(s): 42.50.Hz, 03.67.Bg, 42.50.Dv, 78.67.Hc

I. INTRODUCTION

The search for quantum light sources exhibiting two-photon emission is related directly to applications in quantum information processing, cryptography, and imaging.[1,2] Prominent examples for two-photon emission involve parametric down-conversion and highly pumped semiconductor quantum wells,[3] as well as atomic or semiconductor quantum dot (QD) based four-level systems.[4,5] In contrast to single-photon processes, which are bound to sub-Poissonian distributions, the statistics of a two-photon emission varies from nonclassical (sub-Poissonian) to even chaotic (super-Poissonian) behavior. For example, polarization-entangled photon pairs generated by a light-emitting diode can exhibit a sub-Poissonian distribution.[4,6] However, two-photon emission in the case of single emitters is not always solely associated with sub-Poissonian distributions as shown in the present contribution.

Here, we report on controllable excitonic photon emission statistics from a four-level system, as represented by the biexciton cascade emission from a QD, which is achieved by varying the biexciton binding energy, pump power, and temperature. GaN QDs appear as an ideal semiconductor based candidate for a study of such photon emission statistics because two significant parameters, namely the fine-structure splitting of the excitonic bright states[7] and the biexciton binding energy,[8–10] can efficiently be tuned close to, or even across, zero depending on the QD size. As a result, the photon statistics is drastically altered, which is, e.g., expressed by the observation of a different degree of bunched two-photon emission. Depending on the electronic configuration of the QD, the reported two-photon emission can deteriorate the antibunched single-photon emission property of an exciton as long as the biexciton state is still populated, in addition to, e.g., commonly assumed background luminescences.[11,12] *We experimentally and theoretically show that, depending on the configuration of the QD's electronic states, the number of contributing decay processes changes drastically and shifts the weight between one- and two-photon processes, favoring either antibunched or bunched emission*. Our results contribute to the fundamental understanding of few-photon emission events and demonstrate the importance of measuring the photon statistics in order to probe exciton correlations involved in the emission process. The observed tunable stream of bunched photons is inherently related and applicable to previously as nonclassical considered effects,[13] such as, e.g., subwavelength interference[14] and ghost imaging.[15]

II. EXPERIMENTAL DETAILS

We have investigated self-assembled, low density ($\sim 6 \times 10^9$ cm^{-2}), wurtzite GaN QDs grown by low-pressure metal-organic vapor deposition. After deposition of a 100-nm-thick layer of AlN on top of an *n*-type 6H-SiC [0001] substrate, the GaN QDs were segregated and subsequently capped with another 100 nm of AlN. In order to reduce the observed emission linewidth and to eliminate spectral jitter, the resulting sample was subsequently annealed[16] under a NH_3 flow. A detailed growth description can be found elsewhere.[17–19]

In order to facilitate microphotoluminescence (μPL) measurements the sample was processed by electron-beam lithography into mesa structures with corresponding diameters down to 200 nm. As excitation source for the single QD μPL measurements the 325.0-nm emission line of a HeCd laser was applied and for the temperature-dependent analysis a He-flow cryostat was utilized. μPL spectra were recorded with a UV-enhanced Si–charge-coupled device (CCD) array while measurements of the second-order correlation function ($g^{(2)}$) were performed by bialkali photomultiplier tubes (PMTs) with a biphoton time resolution of 0.35 ns in a Hanbury-Brown and Twiss (HBT) setup.

III. BUNCHING PHENOMENON

Figure 1(a) presents a scheme of the employed HBT correlation setup with indicators for the applied bandpass configurations (I, II, III) and detected excitonic complexes (exciton, X, and/or biexciton, B). The corresponding μPL spectrum of a single GaN QD with X and antibinding B

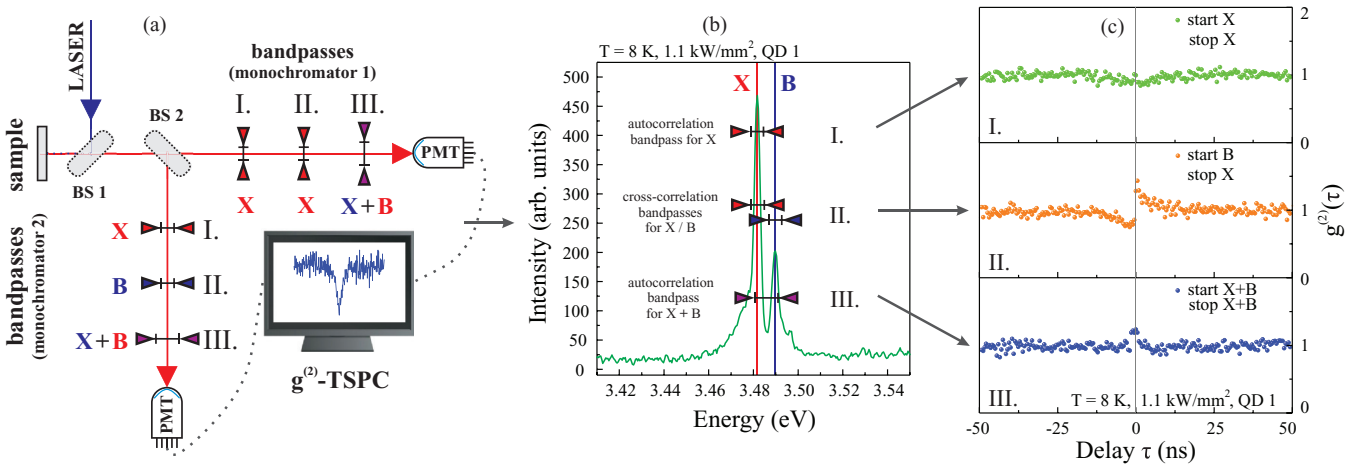

FIG. 1. (Color online) (a) Hanbury-Brown and Twiss setup for photon correlation measurements. Three different bandpass configurations (I, II, III) are illustrated along with the detected excitonic complex (exciton, X, and/or biexciton, B. (b) μPL spectrum of a single GaN quantum dot showing X and antibinding B emission. The spectral width of the bandpasses for the auto- and cross-correlation measurements is depicted. (c) Autocorrelation measurement of X, cross-correlation measurement of B/X, wide bandpass autocorrelation measurement of $X + B$. Bandpass configuration III indicates bunching with $g^{(2)}(0) = 1.23$.

emission is illustrated in Fig. 1(b). Due to a large inscribed dipole moment, single GaN QD emission is affected by spectral diffusion[7,19] and acoustic-phonon coupling.[20] Mainly, the combination of both effects yields the observed full width at half maximum (FWHM) of X and B emission in the meV range, which stands in contrast to the corresponding radiative lifetimes, which are of the order of several ns for QD 1–3 as measured by time resolved μPL measurements (not shown). For instance for QD 1 we obtain a radiative decay time of 7.7 ns for X and 4.4 ns for B. The different applied bandpass configurations correspond to an autocorrelation measurement of X (I), a cross-correlation measurement of B and X (II), and a wide bandpass autocorrelation measurement that collects *both* complexes in *both* detection channels (III). As a result, a weak [$g^{(2)}(0) = 0.90$] antibunching is observed in Fig. 1(c) for the bandpass configuration I. Such an incomplete antibunching feature can be explained as follows: In contrast to a low pump situation exhibiting pronounced antibunching for similar GaN/AlN QDs,[19,21] we not only aim at excitonic emission but also at the influence of the occupied biexciton state on the emission statistics for particular low biexciton binding energies (see Sec. IV for further details). The common signature of a cross-correlation measurement of B and X, i.e., antibunching for negative delay times (τ) followed by bunching for positive τ, appears for bandpass configuration II. In contrast, for the wide bandpass autocorrelation measurement (III) a definite [$g^{(2)}(0) = 1.23$] and around $\tau = 0$ symmetric bunching feature is observed.

In order to explore the origin of this bunching feature we systematically analyzed a large number of single GaN QDs in order to locate QDs with varying biexciton binding energies E^B_{bind} around an emission energy of 3.5 eV. Exemplary μPL spectra of 3 GaN QDs (QDs 1–3) are illustrated in Fig. 2(a). QD 1 exhibits spectrally resolved X and antibinding B emission with a biexciton binding energy of $E^X - E^B = E^B_{\text{bind}} = -8.1$ meV. QDs 2 and 3 exhibit E^B_{bind} below the FWHM of the envelope of the X and B emission. In contrast to QD 1, only one dominant emission line composed by X and B emission is observed. Based on a common FWHM value of $\gtrsim$5.0 meV for X emitting at $\approx$3.5 eV, an estimate of E^B_{bind} can be obtained for QDs 2 and 3, which yields $|E^B_{\text{bind}}| \leqslant |-2.0|$ meV and $|E^B_{\text{bind}}| \leqslant |-0.3|$ meV, respectively. Autocorrelation measurements of the dominant emission of QD 3 with a bandpass as illustrated in Fig. 2(a) allows for the observation of a strong bunching with $g^{(2)}(0) = 3.10$ as shown in Fig. 2(b). An increase of the detuning E^B_{bind} between the X and the B transition via QD 2 towards QD 1 now reduces the observed bunching effect down to $g^{(2)}(0) = 1.23$ as depicted in Fig. 2(b) and later on quantified in Fig. 3(b).

The identification of the emission lines in the μPL spectra [Figs. 1(b) and 2(a)] of the GaN QDs originates from numerous power dependent μPL and $g^{(2)}$-correlation function measurements on spectrally resolved and overlaying exciton (X) and biexction (B) emission peaks as exemplarily represented by QDs 1–3. The comparison of absolute emission line areas in regard to variations of the pump power yields the mean exciton occupation number μ for each excitonic complex.[22] Within the spectral range around 3.5 eV we commonly observe, e.g., $\mu_X = 1.1(1)$ and $\mu_B = 2.0(1)$ for GaN QDs like QD 1, which strongly indicates the identification of X and B emission.[8,23] Also, the typical signature of a cross-correlation measurement as obtained for B and X [Fig. 1(c)] demonstrates a cascade process and hence further supports the given emission line identification.[24]

Before turning towards the interpretation of the bunching phenomenon, we summarize some facts concerning the unusual biexcitonic structure of GaN/AlN QDs in order to substantiate the given emission line assignment. Within the analyzed spectral range at around 3.5 eV it is common for GaN QDs to exhibit the observed antibinding B emission.[8,23] The large spatial separation of the charge carriers in GaN QDs, originating from the built-in polarization fields parallel to the [0001] axis, leads to a reduction of the binding terms in the B complex. For modeling this balance between binding and

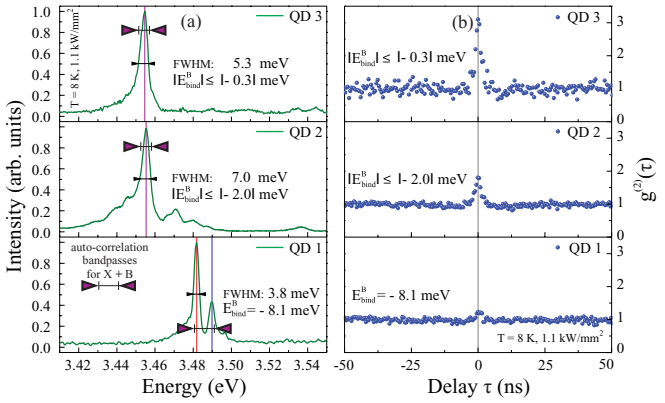

FIG. 2. (Color online) (a) Exemplary μPL spectra of GaN QDs 1–3 showing spectrally resolved exciton (X) and biexciton (B) emission (QD 1) or corresponding spectrally overlapping $X+B$ emission (QDs 2 and 3). The FWHM and the biexciton binding energy (E^B_{bind}) are shown along with applied autocorrelation bandpasses. (b) Autocorrelation measurements for the corresponding QDs illustrate the inverse scaling behavior between the photon bunching strength $g^{(2)}(0)$ and the detuning E^B_{bind}.

antibinding terms in the B complex, the Coulomb, exchange, and correlation interactions need to be taken into account.[10,25] Interestingly, for $\approx 2\%$ of the GaN QDs emitting at around 3.5 eV, as derived from a large (>200) number of μPL measurements, the compensation between the binding and antibinding terms in the B complex leads to a strong reduction of the absolute value of the biexciton binding energy $|E^B_{\text{bind}}|$ as, e.g., observed for QDs 2 and 3. As a consequence no clear spectral separation between the X and B emission lines can be observed within the occurring FWHM and bunching in the $g^{(2)}$-correlation function occurs for selected QDs [cf. Fig. 2(b)]. Our statistical μPL analysis has shown for the analyzed sample that an average $E^B_{\text{bind}} \approx -8$ meV is common for GaN QDs emitting at around 3.5 eV. However, mainly due to diameter fluctuations of the QDs, in our sample one can also observe $|E^B_{\text{bind}}|$ values well below the commonly observed FWHM value of $\gtrsim 5.0$ meV for X. Consequently, power dependent μPL measurements yield mean exciton occupation numbers of $\mu_{X+B} = 1.4(1)$, e.g., for QDs 2 and 3 suggesting a spectral overlay between the X and B emission for those QDs.

IV. QUANTUM-STATE TOMOGRAPHY OF THE BIEXCITON CASCADE

Next, we address the explanation of the observed bunching phenomenon. Bunching in the $g^{(2)}$-correlation function itself is not an uncommon feature in QD spectroscopy and is, e.g., assigned to spectral diffusion[26,27] or an exclusively by biexcitons induced bunching at low pump rates.[28] However, we can exclude such origins for the reported bunching phenomenon based on the discussion in Sec. VIII. Especially the E^B_{bind} dependence of the bunching phenomenon does not allow its straightforward simulation based on typical rate equation approaches[29,30] and realistic parameters for GaN/AlN QDs.[22,31] As a consequence we numerically solved the quantum-state tomography of the biexciton cascade[32,33] in order to also account for the quantum-mechanical particularities of the analyzed system. The corresponding Hamilton operator within the rotating wave and dipole approximation, still without the system-environment coupling, reads

$$H = \hbar \sum_k \omega_k^0 c_k^\dagger c_k - \hbar \sum_{j=H,V} M_k (G^\dagger X_j c_k^\dagger + X_j^\dagger B c_k^\dagger) + \text{H.c.} + \hbar\omega_B\, B^\dagger B + \hbar\omega_H\, X_H^\dagger X_H + \hbar\omega_V\, X_V^\dagger X_V. \quad (1)$$

Here the Coulomb interaction between the horizontally and vertically polarized excitons (H,V) is incorporated in the ground state $G^\dagger$, the exciton $X^\dagger_{H/V}$, and the biexciton $B^\dagger$ operators with the eigenenergies $\hbar\omega_{B/H/V}$, determined by the fine-structure splitting of the excitonic bright states $E^X_{\text{FSS}} = \hbar(\omega_H - \omega_V)$ and E^B_{bind}. The precise value for E^X_{FSS} does not change our theoretical results if chosen as just sufficiently small in comparison to E^B_{bind}, which is typical for GaN QDs emitting at around 3.5 eV.[7] Hence for simplicity we assume $\omega_H = \omega_V$ for the following explanation [cf. Figs. 3(a) and 3(d)]. The ground-state energy is chosen as zero and the electron-photon coupling element M_k couples equally strong to both polarizations (H,V), while the photon creation and annihilation operators are denoted with $c_k^\dagger$ and c_k. The system dynamics based on the Hamiltonian from Eq. (1) describe very complex emission dynamics into free space, i.e., a photon mode continuum with wave number k.[34,35] Since the experiment only detects photons in resonance with the exciton-biexciton state transition ($X^\dagger_{H/V} B$) and ground-exciton state transition ($G^\dagger X_{H/V}$), we reduced the complex dynamics to two modes k_B and k_X. Therefore, we assume only two polarization independent modes in resonance with the exciton-ground state transition $\omega_X^0 = c_0 k_X = \omega_{H/V}$ and the biexciton-exciton state transition $\omega_B^0 = c_0 k_B = \omega_B - \omega_{H/V}$ with the photon creation and annihilation operators $c^\dagger_{X/B}$.

Concerning the loss of photons and excitonic coherence due to the system-environment coupling, we apply a Markovian approximation. This is possible, since the time scale of the observed emission processes leading to a bunching signature is within the nanosecond regime and, clearly, losses such as pure dephasing dominate the dynamics. In order to consistently introduce the losses we choose the Born-Markov approach in the Lindblad form for a system operator A ($\mathcal{L}[A]\rho := 2A\rho A^\dagger - A^\dagger A\rho - \rho A^\dagger A$) and take into account photon mode loss κ, incoherent pumping P,[36] radiative decay Γ_{rad}, and phenomenological pure dephasing γ_{pure} (LA-phonon based, band diagonal pure dephasing mechanism[32]) based on their corresponding rates. Finally, the complete dynamics is calculated within the density matrix ρ approach ($\dot\rho = \frac{i}{\hbar}[\rho, H] + \mathcal{L}\rho$) for parameters in the weak-coupling limit: $\kappa + \gamma_{\text{pure}} \gg M$ in order to prevent any induced emission dynamics, clearly not present in the experiment for the dissipative Liouvillian $\mathcal{L}$. As a result of the introduced simplifications the theoretical description does not allow a full quantitative discussion of the bunching phenomenon, but the approach still provides an essential qualitative description and successfully reveals the underlying physics. We applied the following dissipative

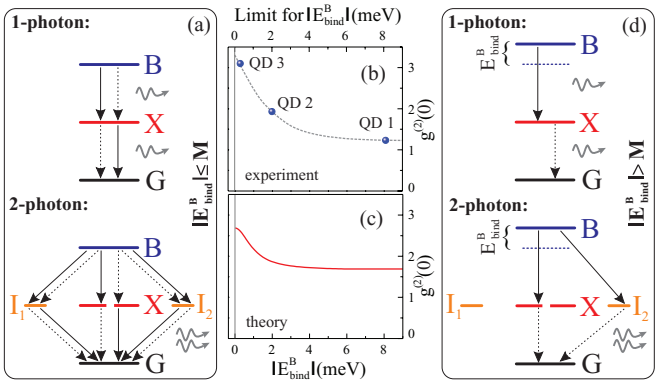

FIG. 3. (Color online) (a) Level scheme of the biexciton cascade for the resonant case with a biexciton binding energy $|E^B_{\text{bind}}| \leqslant M$. Biexciton, exciton, intermediate states, and ground state are denoted with B, X, $I_{1/2}$, and G while M is the electron-photon coupling element. Dashed/solid arrows denote the exciton/biexciton photon modes. (b),(c) Theoretical and experimental $g^{(2)}(0)$ values for varying E^B_{bind} (dashed line is to guide the eye). (d) Level scheme of the biexciton cascade for the nonresonant case $|E^B_{\text{bind}}| > M$.

Liouvillian $\mathcal{L}$:

$$\begin{aligned}\mathcal{L}\rho := \frac{\kappa}{2}\sum_{i=X,B}\mathcal{L}[c_i]\rho + P\sum_{j=H,V}\mathcal{L}[X_j^\dagger G]\rho + \mathcal{L}[B^\dagger X_j]\rho \\ + \Gamma_{\text{rad}}\sum_{j=H,V}\mathcal{L}[G^\dagger X_j]\rho + \mathcal{L}[X_j^\dagger B]\rho \\ - \sum_{k=G,X,B}\gamma_k\left(T_k\rho T_k - \rho\right). \qquad (2)\end{aligned}$$

Here ρ denotes the density matrix while κ, P, Γ_{rad}, and γ_{pure} are the rates for the mode loss, the incoherent pumping,[36,37] the radiative decay, and the phenomenological pure dephasing.[32] The pure dephasing part of $\mathcal{L}$ is defined with $T_G = X_H^\dagger X_H + X_V^\dagger X_V - G^\dagger G$, $T_X = B^\dagger B - X_H^\dagger X_H - X_V^\dagger X_V$, as also $T_B = B^\dagger B - G^\dagger G$ for the three possible population differences and $\gamma_G = \gamma_X = \gamma_{\text{pure}}$, $\gamma_B = 2\gamma_{\text{pure}}$ as the dephasing constants.

Based on the described model we can derive the stationary correlation function $g^{(2)}(0) = \langle c_B^\dagger c_X^\dagger c_X c_B\rangle / \langle c_X^\dagger c_X\rangle\langle c_B^\dagger c_B\rangle$ (see Sec. VI for all resulting equations). Bunching processes, i.e., $g^{(2)}(0) > 1$ [Figs. 2(b) and 3(b)], trivially express that the intensity-intensity correlation (IIC) – two-photon process is greater than the intensity – one-photon process: $\langle c_B^\dagger c_X^\dagger c_X c_B\rangle > \langle c_X^\dagger c_X\rangle\langle c_B^\dagger c_B\rangle$. As a consequence of the measured E^B_{bind} dependence of $g^{(2)}(0)$ [Figs. 2(b) and 3(b)] we now need to elucidate the E^B_{bind} affected balance between the intensity and the IIC. Contributions from all in the generation of the intensity and the IIC involved decay processes facilitates the calculation of $g^{(2)}(0, E^B_{\text{bind}})$ as shown in Fig. 3(c). This theoretical result agrees well with the trend of the experimental data from Fig. 3(b).

V. INTUITIVE EXPLANATION OF THE BUNCHING PHENOMENON

In order to intuitively explain the measured and calculated asymmetric effect of E^B_{bind} on the intensity and the IIC, we now turn to a description of the bunching phenomenon based on the level schemes shown in Figs. 3(a) and 3(d). Here we classify two scenarios with respect to the ratio between the biexciton binding energy E^B_{bind} and the electron-photon coupling element M, the resonant case $|E^B_{\text{bind}}| \leqslant M$ [Fig. 3(a)], and the nonresonant case $|E^B_{\text{bind}}| > M$ [Fig. 3(d)]. Only most dominating, i.e., resonantly contributing, decay processes are depicted with dashed or solid arrows for the exciton and biexciton photon modes k_X and k_B.

The source of the intensity are the photon-assisted B-X and X-G state transitions as depicted in Figs. 3(a) and 3(d) (top). For $|E^B_{\text{bind}}| \leqslant M$ all state transitions are in resonance with the modes of the emitted light field k_X and k_B and hence four transition processes originate the intensity in Fig. 3(a) (top). However, as soon as $|E^B_{\text{bind}}| > M$ occurs, only two processes still resonantly contribute to the intensity as shown in Fig. 3(d) (top), due to the existing mismatch, e.g., between the B-X state transition and the k_X mode.

In contrast to the intensity, the IIC is genuinely a two-photon process, which is first of all fed by a generally larger number of radiative decay processes as illustrated in Figs. 3(a) and 3(d) (bottom). For $|E^B_{\text{bind}}| \leqslant M$ the B-X and X-G state transitions are in resonance with the k_X and k_B modes, and a large number of decay processes arise: The B-X state transition can either populate the one-photon X states (vertical arrows) or the correlated two-photon intermediate (I) states (diagonal arrows), which are either densitylike (I_1) or polarizationlike (I_2) (see Sec. VI for a detailed description). These two-photon I states are a particular feature of the four-level system and are essential for the description of the bunching phenomenon that arises from the biexciton cascade.[6,32] Subsequently, the system evolves via the one-photon X and the intermediate two-photon states I_1 and I_2 into the two-photon G state by emission of a photon pair. As a result there are ten possible two-photon decay processes towards G in Fig. 3(a) (bottom), eight via the two-photon I states and two via the one-photon X state if the weak-coupling regime is assumed. Please note the break in the X state visible in Figs. 3(a) and 3(d) (bottom), which just illustrates that no twofold population of the same mode is possible in the IIC schemes.

Again with a larger detuning $|E^B_{\text{bind}}| > M$ the situation changes significantly. Due to the lifted resonance condition only two two-photon decay processes survive and contribute efficiently to the IIC as expressed by the remaining bunching in Figs. 3(b) and 3(c) for larger detunings. All eight other processes become off-resonant and hence negligible as shown in Fig. 3(d) (bottom). Only one residual process still resonantly populates the polarizationlike two-photon I_2 state and another one the X state, which then allows the formation of a photon pair. *Hence the reduction of the number of contributing decay processes is 10:2 for the IIC, which is in clear contrast to the case of the intensity, where the reduction of the contributing decay processes is just 4:2. This asymmetry in the E^B_{bind} dependence of the $g^{(2)}(0)$ function based on the number of contributing decay channels for the intensity and the IIC explains the detuning dependence of the bunching phenomenon.* Only the absolute detuning value $|E^B_{\text{bind}}|$ is relevant for the steering of the photon statistics between one- and two-photon processes (intensity $\leftrightarrow$ IIC) as the detuning dependence of $g^{(2)}(0)$ is symmetric, i.e., only the energetic difference between $|E^B_{\text{bind}}|$ and M tunes the bunching strength.

Under consideration of the particular nature of a four-level system it is now also possible to understand the comparable[19] weak antibunching feature of the excitonic emission of QD 1 in Fig. 1(c) [$g^{(2)}(0) = 0.90$]. Even though the X and B emission are spectrally separated, there is just weak indication for an antibunching dip due to a residual overlay with the two-photon process induced bunching, which is neglected in frequently applied two-level based models.[21,29,30] Not only, e.g., do commonly assumed background luminescences deteriorate such single-photon emission,[11,12] also two-photon processes play a dominant role if the biexciton state is initially occupied. This matter is demonstrated by the residual bunching in Figs. 3(b) and 3(c), even for larger E^B_{bind} exceeding the FWHM of the related emission lines. For particular large E^B_{bind} of ~ -35 meV,[19] one can observe much smaller $g^{(2)}(0)$ values compared to QD 1 for even up to 200 K due to a negligible influence of two-photon processes, cf. Fig. 3(b). Please note that the theory also predicts a strong influence of E^X_{FSS} on the bunching phenomenon as soon as it approaches the quantity of M. Hence for particular and on the analyzed sample rare QD shapes and sizes it is even possible to observe smaller $g^{(2)}(0)$ values than for QD 1 with comparable E^B_{bind} but consequently deviating and not negligible E^X_{FSS}. By choosing typical GaN/AlN QDs emitting at around 3.5 eV, based on analyzing a statistical valid number of QDs, one frequently observes QDs with negligible E^X_{FSS} in regard to M and E^B_{bind}. Hence for smaller GaN/AlN quantum dots emitting at higher energies or even for on other material system based QDs as, e.g., InAs/GaAs QDs, one would have to take the unique balance of E^B_{bind} and E^X_{FSS} into account in order to estimate the strength of the two-photon processes that induce the bunching phenomenon.

VI. ONE- AND TWO-PHOTON PROCESSES IN THE BIEXCITON CASCADE

The explanation of the bunching phenomenon is mainly based on the number of decay processes, which either contribute to the intensity or the intensity-intensity-corellation (IIC) representing the denominator and nominator of the $g^{(2)}$-correlation function, respectively. We distinguish between the resonant case $|E^B_{\text{bind}}| \leqslant M$ and the nonresonant case $|E^B_{\text{bind}}| > M$ by comparing $|E^B_{\text{bind}}|$ with the electron-photon coupling element M. Even though the given explanation based on level schemes [Figs. 3(a) and 3(d)] might be intuitive, it cannot account for all the details of such a complex four-level system as the biexciton cascade. In detail we can, e.g., describe the level schemes, which illustrate the generation of the intensity (one-photon processes) in Figs. 3(a) and 3(d) (top) via the decay of the biexciton density $\langle B^\dagger B\rangle$ by spontaneous emission as shown in the following:

$$
\begin{aligned}
&(1) \quad \langle B^\dagger B\rangle \xrightarrow{\Delta} \langle X^\dagger B c_X^\dagger\rangle \xrightarrow{\Delta} \langle c_X^\dagger c_X\rangle,\\
&(2) \quad \langle B^\dagger B\rangle \rightarrow \langle X^\dagger B c_B^\dagger\rangle \rightarrow \langle c_B^\dagger c_B\rangle,\\
&(3) \quad \langle X^\dagger X\rangle \xrightarrow{\Delta} \langle G^\dagger X c_B^\dagger\rangle \xrightarrow{\Delta} \langle c_B^\dagger c_B\rangle,\\
&(4) \quad \langle X^\dagger X\rangle \rightarrow \langle G^\dagger X c_X^\dagger\rangle \rightarrow \langle c_X^\dagger c_X\rangle.
\end{aligned}
$$

Decay paths 1 and 3 (black) are influenced by the absolute value of a detuning $\Delta = |E^B_{\text{bind}}|$ and vanish for rising $|E^B_{\text{bind}}|$, whereas decay paths 2 and 4 (red) are maintained even for larger detunings. Here the ground state, the exciton, and the biexciton operators are denoted by $G^\dagger$, $X^\dagger$, and $B^\dagger$, while the photon creation and annihilation operators are denoted by $c^\dagger_{X/B}$ and $c_{X/B}$. For the resonant case all four decay processes contribute to the intensity but as soon as the nonresonant case is reached, only two decay processes remain and contribute to the denominator of the $g^{(2)}$-correlation function. However, for the IIC as the numerator of the $g^{(2)}$-correlation function, ten decay processes contribute to the resonant case that is reduced to two dominant decay processes (red) for the nonresonant case with larger detuning $\Delta = E^B_{\text{bind}}$. The resulting decay processes (two-photon processes) for the IIC are illustrated in Figs. 3(a) and 3(d) (bottom) and can be summarized to

$$
\begin{aligned}
&(1) : I_2 \quad \langle B^\dagger B\rangle \xrightarrow{\Delta} \langle X^\dagger B c_X^\dagger\rangle \xrightarrow{\Delta} \langle G^\dagger B c_X^\dagger c_B^\dagger\rangle\\
&\qquad \xrightarrow{\Delta} \langle G^\dagger X c_X^\dagger c_B^\dagger c_X\rangle \xrightarrow{\Delta} \langle c_B^\dagger c_X^\dagger c_X c_B\rangle,\\
&(2) : I_2 \quad \langle B^\dagger B\rangle \xrightarrow{\Delta} \langle X^\dagger B c_X^\dagger\rangle \xrightarrow{\Delta} \langle G^\dagger B c_X^\dagger c_B^\dagger\rangle\\
&\qquad \rightarrow \langle G^\dagger X c_X^\dagger c_B^\dagger c_B\rangle \rightarrow \langle c_B^\dagger c_X^\dagger c_X c_B\rangle,\\
&(3) : X \quad \langle B^\dagger B\rangle \xrightarrow{\Delta} \langle X^\dagger B c_X^\dagger\rangle \xrightarrow{\Delta} \langle X^\dagger X c_X^\dagger c_X\rangle\\
&\qquad \xrightarrow{\Delta} \langle G^\dagger X c_X^\dagger c_B^\dagger c_X\rangle \xrightarrow{\Delta} \langle c_B^\dagger c_X^\dagger c_X c_B\rangle,\\
&(4) : I_1 \quad \langle B^\dagger B\rangle \xrightarrow{\Delta} \langle X^\dagger B c_X^\dagger\rangle \rightarrow \langle X^\dagger X c_X^\dagger c_B\rangle\\
&\qquad \rightarrow \langle G^\dagger X c_X^\dagger c_B^\dagger c_X\rangle \xrightarrow{\Delta} \langle c_B^\dagger c_X^\dagger c_X c_B\rangle,\\
&(5) : I_1 \quad \langle B^\dagger B\rangle \xrightarrow{\Delta} \langle X^\dagger B c_X^\dagger\rangle \rightarrow \langle X^\dagger X c_X^\dagger c_B^\dagger\rangle\\
&\qquad \xrightarrow{\Delta} \langle G^\dagger X c_X^\dagger c_B^\dagger c_B\rangle \rightarrow \langle c_B^\dagger c_X^\dagger c_X c_B\rangle,\\
&(6) : I_2 \quad \langle B^\dagger B\rangle \rightarrow \langle X^\dagger B c_B^\dagger\rangle \rightarrow \langle G^\dagger B c_X^\dagger c_B^\dagger\rangle\\
&\qquad \xrightarrow{\Delta} \langle G^\dagger X c_X^\dagger c_B^\dagger c_X\rangle \xrightarrow{\Delta} \langle c_B^\dagger c_X^\dagger c_X c_B\rangle,\\
&(7) : I_2 \quad \langle B^\dagger B\rangle \rightarrow \langle X^\dagger B c_B^\dagger\rangle \rightarrow \langle G^\dagger B c_X^\dagger c_B^\dagger\rangle\\
&\qquad \rightarrow \langle G^\dagger X c_X^\dagger c_B^\dagger c_B\rangle \rightarrow \langle c_B^\dagger c_X^\dagger c_X c_B\rangle,\\
&(8) : X \quad \langle B^\dagger B\rangle \rightarrow \langle X^\dagger B c_B^\dagger\rangle \rightarrow \langle X^\dagger X c_B^\dagger c_B\rangle\\
&\qquad \rightarrow \langle G^\dagger X c_X^\dagger c_B^\dagger c_B\rangle \rightarrow \langle c_B^\dagger c_X^\dagger c_X c_B\rangle,\\
&(9) : I_1 \quad \langle B^\dagger B\rangle \rightarrow \langle X^\dagger B c_B^\dagger\rangle \xrightarrow{\Delta} \langle X^\dagger X c_X^\dagger c_B\rangle\\
&\qquad \xrightarrow{\Delta} \langle G^\dagger X c_X^\dagger c_B^\dagger c_B\rangle \rightarrow \langle c_B^\dagger c_X^\dagger c_X c_B\rangle,\\
&(10) : I_1 \quad \langle B^\dagger B\rangle \rightarrow \langle X^\dagger B c_B^\dagger\rangle \xrightarrow{\Delta} \langle X^\dagger X c_X^\dagger c_B\rangle\\
&\qquad \rightarrow \langle G^\dagger X c_X^\dagger c_B^\dagger c_X\rangle \xrightarrow{\Delta} \langle c_B^\dagger c_X^\dagger c_X c_B\rangle.
\end{aligned}
$$

As an example for the resulting complex set of equations of motions we list the equation of motion for the photon-assisted ground-biexciton state transition:

$$
\begin{aligned}
&\partial_t \left\langle G^\dagger B C_B^{m,n} C_X^{p,q}\right\rangle\\
&\quad = -i\left(\omega_B - (m-n)\omega_B^0 - (p-q)\omega_X^0\right)\left\langle G^\dagger B C_B^{m,n} C_X^{p,q}\right\rangle\\
&\qquad - \kappa(m+n+p+q)\left\langle G^\dagger B C_B^{m,n} C_X^{p,q}\right\rangle\\
&\qquad - (2P + 2\gamma_{\text{pure}} + 2\Gamma_{\text{rad}})\left\langle G^\dagger B C_B^{m,n} C_X^{p,q}\right\rangle\\
&\qquad + i\,M \sum_{i=H,V} \left\langle X_i^\dagger B\, C_B^{m,n+1} C_X^{p,q}\right\rangle + \left\langle X_i^\dagger B\, C_B^{m,n} C_X^{p,q+1}\right\rangle
\end{aligned}
$$

$$-i\,M\sum_{i=H,V}\left\langle G^{\dagger}X_i\;C_B^{m,n+1}C_X^{p,q}\right\rangle+\left\langle G^{\dagger}X_i\;C_B^{m,n}C_X^{p,q+1}\right\rangle$$
$$+i\,M\sum_{i=H,V}m\left\langle X_i^{\dagger}B\;C_B^{m-1,n}C_X^{p,q}\right\rangle+p\left\langle X_i^{\dagger}B\;C_B^{m,n}C_X^{p-1,q}\right\rangle \tag{3}$$

with $C_B^{m,n}:=c_B^{\dagger m}c_B^n$ and $C_X^{p,q}:=c_X^{\dagger p}c_X^q$ and m,n,p,q as integers. Since we calculate the observable in the spontaneous emission limit, only ground-biexciton state transitions with $m+p=2$ and $n=q=0$ contribute. Equation (4) exemplarily shows the resulting important polarizationlike intermediate state transition with $m=2$, $p=0$:

$$\begin{aligned}\partial_t\left\langle G^{\dagger}BC_B^{2,0}C_X^{0,0}\right\rangle&=-i\left(\omega_B-2\omega_B^0\right)\left\langle G^{\dagger}BC_B^{2,0}C_X^{0,0}\right\rangle\\&\quad-2(\kappa+P+\gamma_{\text{pure}}+\Gamma_{\text{rad}})\left\langle G^{\dagger}BC_B^{2,0}C_X^{0,0}\right\rangle\\&\quad+i\,2\,M\sum_{i=H,V}\left\langle X_i^{\dagger}B\;C_B^{1,0}C_X^{0,0}\right\rangle.\end{aligned}$$

Finally, we are interested in the stationary, adiabatic limit and write the biexciton energy as $\omega_B=\omega_B^0+\omega_X^0$ in order to obtain

$$\left\langle G^{\dagger}BC_B^{2,0}C_X^{0,0}\right\rangle=i\,2\,M\sum_{i=H,V}\frac{\left\langle X_i^{\dagger}B\;C_B^{1,0}C_X^{0,0}\right\rangle}{iE_{\text{bind}}^B+2(\kappa+P+\gamma_{\text{pure}}+\Gamma_{\text{rad}})}. \tag{5}$$

Note: $\omega_B-2\omega_B^0=\omega_B^0+\omega_X^0-2\omega_B^0=\omega_X^0-\omega_B^0=-E_{\text{bind}}^B$ with $\omega_B^0=\omega_X^0+E_{\text{bind}}^B$. Consequently, for this important transition that is feeding the cross correlation, we observe a strong effect of E_{bind}^B and γ_{pure}, which is for the latter case twice as large as for the one-photon transitions. The full set of parameters used for the calculation of the bunching phenomenon and its E_{bind}^B, pump rate and temperature dependence is listed in Table I.

The two remaining decay processes 7 and 8 (red) for the nonresonant case decay via the polarizationlike two-photon intermediate I_2 and the X state and are not effectively affected by the detuning $\Delta=E_{\text{bind}}^B$, cf. Fig. 3(d) (bottom). The decay processes via the intermediate two-photon I_1 or I_2 states are either densitylike or polarizationlike, as expressed by the notation of the processes given in either 4, 5, 9, and 10 or 1, 2, 6, and 7. Processes 3 and 8 represent decay processes via the X state and are classical in the case of 8 (first generation of a B photon then of an X photon) or clearly nonclassical as for case 3 (first generation of an X photon then of a B photon). Please note that only the absolute value of the detuning $\Delta=|E_{\text{bind}}^B|$ has an impact on the contribution of the decay processes to the intensity and the IIC as only the energetic state offset influences the computed dynamics.

TABLE I. Set of essential parameters applied for the quantum-state tomography calculations of the biexciton cascade in wurtzite GaN quantum dots.

Parameter description	Value
electron-photon coupling element M	0.06 ps^{-1}
pump rate P	$M\times0.025$
mode loss rate κ	$M\times16$
radiative decay rate Γ_{rad}	1.5 ns^{-1}
pure dephasing rate γ_{pure}	0.32 ps^{-1}
fine-structure splitting E_{FSS}^X	4 μeV

VII. PUMP POWER AND TEMPERATURE DEPENDENCE

Further parameter studies of the pump power and the temperature dependence were conducted in order to confirm the given interpretation by a comparison of the trends for the experimentally and theoretically derived $g^{(2)}(0)$ values. Figure 4(a) illustrates the power dependence of the bunching phenomenon for QD 2 at 25 K, showing a reduction of the bunching towards higher pump powers [Fig. 4(b)]. The evolution of the bunching phenomenon with temperature is shown in Fig. 4(c). At 6 K a strong bunching is observed for QD 2, which is reduced upon the rise of temperature towards 50 K and finally vanishes at $\leqslant$ 70 K [Fig. 4(d)]. For the smallest in the experiment reached pump powers and temperatures, two-photon processes can well compete

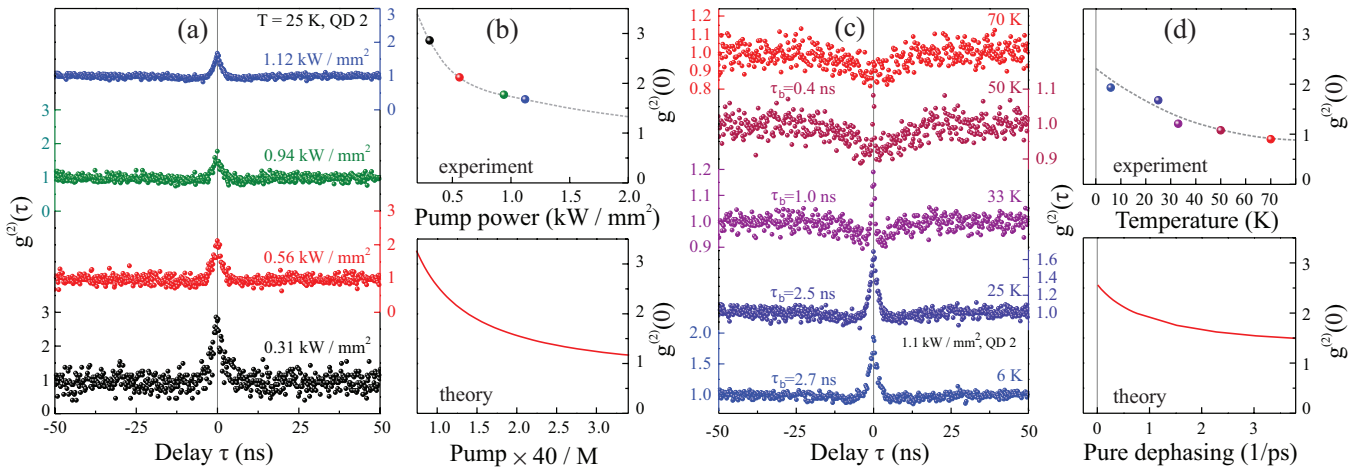

FIG. 4. (Color online) (a) Power dependence of the $g^{(2)}$-correlation function for QD 2 at 25 K. (b) Power dependence of the $g^{(2)}(0)$ values. (c) Temperature dependence of the bunching phenomenon up to 70 K. The $g^{(2)}(0)$ value is reduced while the bunching FWHM narrows (τ_b). (d) Temperature dependence of the $g^{(2)}(0)$ values. Dashed lines are guides to the eye.

with one-photon processes. Consequently, a bunched photon emission is observed as long as the biexciton state is still sufficiently populated.

Both the pump power and the temperature dependence of the bunching phenomenon can be understood within the framework of our model if the pure and the excitation induced dephasing are considered. Most two-photon processes, which, i.a., relax via the intermediate I states, are twice as sensitive[36,37] to such dephasings ($-2\gamma_{\text{pure}}$, $-2P$) in regard to their one-photon counterparts (see Sec. VI). Hence an increased pumping or temperature simply reduces the number of participating two-photon decay processes more drastically, if compared to the one-photon case, in accordance with the E^B_{bind} detuning dependence, cf. Fig. 3. The measured $g^{(2)}(0)$ dependencies are in good qualitative agreement with the corresponding theoretical results in Figs. 4(b) and 4(d), which well support the given interpretation. The rising temperature also strongly affects the FWHM of the bunching peak τ_b, which is reduced from 2.7 to 0.4 ns in the temperature interval from 6 to 50 K, cf. Fig. 4(c). This speeding up of the bunching phenomenon demonstrates the rapid dephasing of the two-photon process by acoustic phonons, while the one-photon process remains stable up to 70 K [Fig. 4(c)] and above in GaN QDs[19] due to a deep confinement potential.

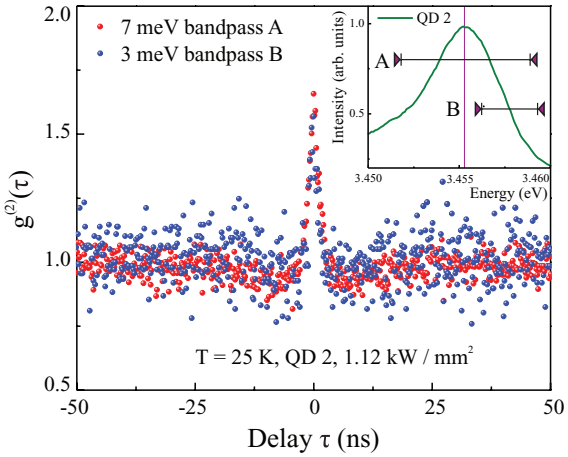

FIG. 5. (Color online) Autocorrelation measurements of QD 2 based on different bandpass configurations (A and B) with varying spectral widths (7 and 3 meV) and position as illustrated in the inset showing the related μPL spectrum. Altering the bandpass configuration does not drastically affect the bunching signature, which allows us to exclude spectral diffusion as the origin of the bunching phenomenon.

VIII. DISCUSSION

The given interpretation of the bunching phenomenon well explains its biexciton binding energy, pump power and temperature dependencies and is further supported by the detailed emission line identification. However, bunching in the $g^{(2)}$-correlation function can also occur mainly due to the following two alternative effects that must be ruled out in order to proof the reported observation of two-photon emission based bunching.

First, spectral diffusion as origin of the reported bunching phenomenon must be excluded. Due to the huge built-in dipole moments in wurtzite GaN QDs up to $2e \times$ nm and a surrounding defect rich AlN matrix material one observes a drastic emission line broadening. The defect rich AlN matrix material induces a fluctuating Coulomb field in the vicinity of a GaN QD that constantly alters the emission energy of the inherent excitonic complexes. As a result, spectral emission line jitter, emission line broadening,[20] and a particular power dependence of the emission linewidths[22,38] can be observed.

Figure 5 shows autocorrelation measurements of the bunched emission from QD 2 for two bandpass configurations A and B as illustrated in the inset. Commonly, such variation of the applied bandpass widths and spectral positions drastically alters the strength of the bunching if originated by spectral diffusion.[26,27] For a bandpass configuration comprising the full QD emission (bandpass A), a comparably weak bunching should occur in case of spectral diffusion on a ns time scale. In contrast, the bunching in the $g^{(2)}$-correlation function should strengthen as soon as the bandpass width for the autocorrelation measurement is reduced and spectrally shifted towards coverage of one half of the emission line (bandpass B). Due to the limited spectral diffusion time the, e.g., excitonic emission remains in the energy range of bandpass B for a time period in access of the radiative decay time, which results in a bunched photon stream. However, altering the bandpasses does not drastically affect the bunching strength or the general shape of the $g^{(2)}$-correlation function as shown in Fig. 5. This observation confirms that the homogeneous emission line does not remain within one half of the broadened emission line on a ns time scale. For bandpass B we even observe a weak reduction of the bunching phenomenon in Fig. 5 due to the residual small spectral separation between the X and B emission for QD 2, cf. Fig. 3(b). Hence the observed bunching phenomenon for QD 1–3 does not originate from spectral diffusion.

However, as a second alternative interpretation one needs to consider that even spectrally pure biexcitonic emission can originate a bunching in the $g^{(2)}$-correlation function for low pump powers as shown by Kiraz *et al.*[28] Although the emission line assignment contradicts the observation of purely biexcitonic emission for QDs 2 and 3, we discuss this matter in order to further support the interpretation of the bunching phenomenon as a particular overlay between one- and two-photon processes. An exclusively by biexcitons induced bunching in the $g^{(2)}$-correlation function occurs at $\tau \neq 0$ and is commonly overlaid by a temporarily narrower antibunching feature at $\tau = 0$ in contrast to the results for, e.g., QD 2, cf. Fig. 5. The experimental observation of a biexciton induced bunching at low pump powers[28] can well be modeled based on rate equations for X and B emission,[22] yielding a most pronounced bunching at $\tau \neq 0$, whereas the maximum in the $g^{(2)}$-correlation function for the reported bunching phenomenon occurs at $\tau = 0$, cf. Fig. 5. One could argue that due to the limited time resolution of the applied HBT setup the antibunching dip in the $g^{(2)}$-correlation function measurement of B could be omitted. However, a variation of the pump power commonly tunes the temporal width of an antibunching trace,[21,22] which is not evident in Fig. 4(a) and has never been observed in this study. Hence a purely biexcitonic origin of the bunching phenomenon must be excluded and clearly separated

from the given interpretation based on varying numbers of one- and two-photon processes.

Furthermore, none of the alternative interpretations for the experimental results, namely spectral diffusion and a purely by biexcitonic emission induced bunching in the $g^{(2)}$-correlation function at $\tau \neq 0$, explain the particular biexciton binding energy dependence of the bunching phenomenon.

IX. CONCLUSION

In summary, we have shown that the two-photon emission from the biexciton cascade of a single quantum dot, as representative of a four-level system, can exhibit a super-Poissonian photon distribution in contrast to the sub-Poissonian statistics of, e.g., polarization-entangled photon pairs.[4,6] In particular, we demonstrated experimentally and theoretically how bunched two-photon emission from a single quantum dot can be tuned by means of the biexciton binding energy, pump power, and temperature up to 50 K. Variation of these parameters enables control over the emission from sub-Poissonian one- to super-Poissonian two-photon processes, as explicitly expressed by the reported bunching phenomenon. Alternative common interpretations for a bunching signature in the $g^{(2)}$-correlation function based on purely biexcitonic single-photon emission or spectral diffusion have been ruled out demonstrating the importance of two-photon processes in the biexciton cascade. Moreover, we outlined that the antibunching in the $g^{(2)}$-correlation function of a "single" photon emitter can be overlaid by the reported bunched two-photon process as long as the biexciton state is still populated. Our results prove that the full nature of the four-level system must not be neglected as in two-level based approaches, which evidently only consider one-photon processes.

ACKNOWLEDGMENTS

This work was supported by the Deutsche Forschungsgemeinschaft within the SFB 787 "Halbleiter-Nanophotonik" and the Special Coordination Fund for Promoting Science and Technology of the Japanese Ministry of Education.

*callsen@tu-berlin.de

[1] P. Zoller, T. Beth, D. Binosi, R. Blatt, H. Briegel, D. Bruss, T. Calarco, J. I. Cirac, D. Deutsch, and J. Eisert, Eur. Phys. J. D **36**, 203 (2005).

[2] D. V. Strekalov, A. V. Sergienko, D. N. Klyshko, and Y. H. Shih, Phys. Rev. Lett. **74**, 3600 (1995).

[3] A. Hayat, A. Nevet, P. Ginzburg, and M. Orenstein, Semicond. Sci. Technol. **26**, 083001 (2011).

[4] R. M. Stevenson, C. L. Salter, J. Nilsson, A. J. Bennett, M. B. Ward, I. Farrer, D. A. Ritchie, and A. J. Shields, Phys. Rev. Lett. **108**, 040503 (2012).

[5] D. J. Gauthier, Q. Wu, S. E. Morin, and T. W. Mossberg, Phys. Rev. Lett. **68**, 464 (1992).

[6] Y. Ota, S. Iwamoto, N. Kumagai, and Y. Arakawa, Phys. Rev. Lett. **107**, 233602 (2011).

[7] C. Kindel, S. Kako, T. Kawano, H. Oishi, Y. Arakawa, G. Hönig, M. Winkelnkemper, A. Schliwa, A. Hoffmann, and D. Bimberg, Phys. Rev. B **81**, 241309(R) (2010).

[8] D. Simeonov, A. Dussaigne, R. Butté, and N. Grandjean, Phys. Rev. B **77**, 075306 (2008).

[9] S. Tomić and N. Vukmirović, Phys. Rev. B **79**, 245330 (2009).

[10] S. Tomić and N. Vukmirović, Phys. Rev. B **86**, 159902(E) (2012).

[11] M. D. Wissert, B. Rudat, U. Lemmer, and H. J. Eisler, Phys. Rev. B **83**, 113304 (2011).

[12] M. M. Pelton, C. C. Santori, J. J. Vucković, B. B. Zhang, G. S. G. Solomon, J. J. Plant, and Y. Y. Yamamoto, Phys. Rev. Lett. **89**, 233602 (2002).

[13] A. Nevet, A. Hayat, P. Ginzburg, and M. Orenstein, Phys. Rev. Lett. **107**, 253601 (2011).

[14] J. Xiong, D. Z. Cao, F. Huang, H. G. Li, X. J. Sun, and K. Wang, Phys. Rev. Lett. **94**, 173601 (2005).

[15] F. Ferri, D. Magatti, A. Gatti, M. Bache, E. Brambilla, and L. A. Lugiato, Phys. Rev. Lett. **94**, 183602 (2005).

[16] T. Kawano, S. Kako, C. Kindel, and Y. Arakawa, in *Nano-Optoelectronics Workshop, 2007. i-NOW'07. International* (IEEE, New York, 2007), pp. 120–121.

[17] K. Hoshino, S. Kako, and Y. Arakawa, Appl. Phys. Lett. **85**, 1262 (2004).

[18] M. Miyamura, K. Tachibana, and Y. Arakawa, Appl. Phys. Lett. **80**, 3937 (2002).

[19] S. Kako, C. Santori, K. Hoshino, S. Goetzinger, Y. Yamamoto, and Y. Arakawa, Nat. Mater. **5**, 887 (2006).

[20] I. A. Ostapenko, G. Hönig, S. Rodt, A. Schliwa, A. Hoffmann, D. Bimberg, M. R. Dachner, M. Richter, A. Knorr, S. Kako, and Y. Arakawa, Phys. Rev. B **85**, 081303(R) (2012).

[21] C. Santori, S. Götzinger, Y. Yamamoto, S. Kako, K. Hoshino, and Y. Arakawa, Appl. Phys. Lett. **87**, 051916 (2005).

[22] C. H. Kindel, Ph.D. thesis, University of Tokyo, 2010.

[23] S. Amloy, K. H. Yu, K. F. Karlsson, R. Farivar, T. G. Andersson, and P. O. Holtz, Appl. Phys. Lett. **99**, 251903 (2011).

[24] C. Kindel, S. Kako, T. Kawano, H. Oishi, and Y. Arakawa, Jpn. J. Appl. Phys. **48**, 04C116 (2009).

[25] S. Tomić and N. Vukmirović, Phys. Rev. B **79**, 245330 (2009).

[26] G. Sallen, A. Tribu, T. Aichele, R. André, L. Besombes, C. Bougerol, M. Richard, S. Tatarenko, K. Kheng, and J.-P. Poizat, Nat. Photon. **4**, 696 (2010).

[27] W. Walden-Newman, I. Sarpkaya, and S. Strauf, Nano Lett. **12**, 1934 (2012).

[28] A. Kiraz, S. Fälth, C. Becher, B. Gayral, W. V. Schoenfeld, P. M. Petroff, L. Zhang, E. Hu, and A. Imamoğlu, Phys. Rev. B **65**, 161303 (2002).

[29] P. Michler, A. Imamoğlu, M. D. Mason, P. J. Carson, G. F. Strouse, and S. K. Buratto, Nature (London) **406**, 968 (2000).

[30] E. Moreau, I. Robert, L. Manin, V. Thierry-Mieg, J. M. Gérard, and I. Abram, Phys. Rev. Lett. **87**, 183601 (2001).

[31] S. Kako, Ph.D. thesis, University of Tokyo, 2007.

[32] A. Carmele and A. Knorr, Phys. Rev. B **84**, 075328 (2011).

[33] A. Carmele, F. Milde, M. R. Dachner, M. B. Harouni, R. Roknizadeh, M. Richter, and A. Knorr, Phys. Rev. B **81**, 195319 (2010).

[34] E. del Valle, A. Gonzalez-Tudela, F. P. Laussy, C. Tejedor, and M. J. Hartmann, Phys. Rev. Lett. **109**, 183601 (2012).

[35]J. Kabuss, A. Carmele, M. Richter, and A. Knorr, Phys. Rev. B **84**, 125324 (2011).

[36]H. Carmichael, *Statistical Methods in Quantum Optics 1—Master Equation and Fokker-Planck Equations* (Springer, Berlin Heidelberg New York, 1999).

[37]C. W. Gardiner and P. Zoller, *Quantum Noise* (Springer-Verlag, Berlin Heidelberg New York, 2004).

[38]A. Berthelot, I. Favero, G. Cassabois, C. Voisin, C. Delalande, P. Roussignol, R. Ferreira, and J. M. Gérard, Nat. Phys. **2**, 759 (2006).